Research Article

Copper Adsorption Using Hydroxyapatite Derived from Bovine Bone

Lingchang Kong,[1] Xin Liu [1] Guocheng Lv,[1] Tianming Liu,[2] Peijun Zhang,[1] Yuxin Li,[1] Bin Chen,[3] and Libing Liao [1]

[1]*Beijing Key Laboratory of Materials Utilization of Nonmetallic Minerals and Solid Wastes,*
 National Laboratory of Mineral Materials, School of Material Sciences and Technology, China University of Geosciences,
 Beijing 100083, China
[2]*School of Science, China University of Geosciences, Beijing 100083, China*
[3]*Institute of Environment Engineering, Beijing General Research Institute of Mining & Metallurgy, Beijing 100160, China*

Correspondence should be addressed to Xin Liu; xliu@cugb.edu.cn and Libing Liao; clayl@cugb.edu.cn

Mining and smelting effluent have resulted in heavy metal-contaminated groundwater. Copper-polluted groundwater poses a severe threat to human health and the ecological environment. Permeable reactive barrier (PRB) has been rapidly developed as the in situ remediation technology to control toxic copper migration. Low cost, seepage stability, and great longevity are considered within PRB reactive media. In this paper, hydroxyapatite derived from bovine bone was proven to be a suitable adsorbent owing to cost-effectiveness, great adsorption capacity, and longevity. Batch experiments were carried out to determine the copper adsorption behavior as a function of copper concentration and contact time. Adsorption isotherm was represented by the Langmuir isotherm model, and the adsorption capacity of 25.7 mg/g was superior to most of the adsorbents. A kinetic study was accurately fitted by the pseudo-second-order kinetic model interpreted as a chemical reaction. In addition, the column study confirmed hydroxyapatite has excellent hydraulic performance with no clogging phenomenon happened. At $C/C_0 = 0.5$, the number of pore volume (PV) reached 450. The batch and column experiments also revealed that the overall adsorption process followed up the monolayer chemisorption. Furthermore, systematic analyses demonstrated that surface adsorption was responsible for the copper removal by hydroxyapatite based on experimental analysis and density functional theory (DFT) calculations. This work provides an alternative strategy as filling material for in situ remediation of copper-contaminated groundwater and enriches relevant theoretical references.

1. Introduction

Groundwater is essential for human life and industrial production as a vital water resource [1]. Nowadays, mining and smelting effluent have resulted in more and more heavy metal-contaminated groundwater [2, 3]. Among the toxic heavy metals, copper has posed a severe threat to human health and the natural ecosystem because of accumulation and degradation resistance [4]. The copper concentration is in the range of 1.2 mg/L–200 mg/L under acid mine drainage and polluted groundwater [5, 6]. The copper concentration even reached 1000 mg/L in industrial wastewater [7].

However, the maximum copper concentration of direct discharge is 0.1–0.5 mg/L in different wastewater discharge standards [8, 9]. Hence, efficient remediation of heavy metal polluted groundwater has attracted extensive attention worldwide [10]. Various technologies aim to address this problem, including ex situ remediation using a pump-and-treat (P&T) system or in situ remediation through the permeable reactive barrier (PRB) [11, 12]. P&T technology has been widely used for controlling contaminant migration, but the complicated management, lack of long-term operation, and secondary pollution have remained unsolved [13]. In contrast, PRB technology has been proven to be a

promising strategy due to its cost-effectiveness and sustainability [14]. Thus, PRB was rapidly developed as the green technology for remediating polluted groundwater. The contaminant was immobilized by the reactive media in the filling well through precipitation, adsorption, or reduction into a low-toxicity pollutant [15]. Therefore, the research on filling material for PRB is crucial for heavy metal polluted groundwater [16].

High porosity, effect-cost, seepage stability, and longevity of filling media have been increasingly considered for practical application at pilot or field-scale [17]. Zero-valent iron material is widely applied to PRB due to its outstanding reductivity and adsorption performance [18], but easy oxidation and blocking inhibit its application. Nowadays, studies on natural waste resources as PRB reactive material have developed into hot points. Compared with the expensive synthetic methods, hydroxyapatite derived from animal bone, such as fish bone, chicken bone, and bovine bone, has been developed as an adsorbent for heavy metal polluted water or soil because of its porous structure and excellent adsorption capacity [19–29]. The previous finding suggested that hydroxyapatite could serve for heavy metal-contaminated groundwater, such as uranium, lead, manganese, and copper [30–33]. However, study has not involved in the laboratory column experiment, especially copper flow and transport on hydroxyapatite. Laboratory column experiment could simulate the groundwater condition to explore the flow and pollutant transport model in porous media [34].

Crystallinity plays an important role in the adsorption performance of heavy metals by hydroxyapatite [35]. The previous finding revealed that crystallinity or morphology can be affected by sintering temperature, especially for animal bone [36]. Under low temperatures ($<\sim 600^{\circ}C$), because organic components in the animal bone cannot be completely thermal decomposed, hydroxyapatite derived from the animal bone has low crystallinity with poor mechanical strength; however, it has higher adsorption capacity (e.g., 99.98 mg/g at $400^{\circ}C$) [37, 38]. Under high temperatures ($>\sim 600^{\circ}C$), hydroxyapatite has higher crystallinity with excellent mechanical strength; however, it has lower adsorption capacity [39]. Hydroxyapatite would transform into oxy-hydroxyapatite through dehydroxylation and even decomposed into calcium phosphate with higher sintering temperatures ($>1000^{\circ}C$) [40, 41]. The systematic effect of mechanical strength, pore structure, and adsorption capacity should be comprehensively taken into account in determining the suitable temperature. Therefore, it is essential to investigate the effect of interaction between crystallinity and calcination temperature on copper removal by hydroxyapatite [42].

It was believed that hydroxyapatite has a significant effect on remediation of heavy metal polluted water or soil, and the removal mechanism has been extensively studied [43]. The previous studies demonstrated that surface adsorption was mainly attributable to favorable interaction with the functional group on the surface of hydroxyapatite, such as hydroxyl and phosphate [44, 45]. However, the comprehensive explanation of adsorption sites not be fully revealed completely through traditional analyses [46–48]. Hence, the detailed model with a specific binding site is the key to interpret

adsorption process. Simulation calculation was extensively used to study the adsorption behavior on the surface of hydroxyapatite as supplementary approach [49–51].

In this paper, batch and column experiments were designed to investigate the adsorption performance of copper by hydroxyapatite derived from the bovine bone. The adsorption mechanism was studied in-depth through the experimental analysis methods, such as X-ray diffraction (XRD) combined with Rietveld refinement [52, 53], X-ray photoelectron spectroscopy (XPS), high-resolution transmission electron microscope (HRTEM), and DFT calculations. This work provides the primary reference for evaluating the copper removal mechanism on hydroxyapatite as reactive media within PRB for groundwater remediation.

2. Materials and Methods

2.1. Reagents. Copper nitrate ($Cu(NO_3)_2 \cdot 2H_2O$) used in these experiments was supplied by West Long Chemical Co., Ltd. Copper standard solution was purchased from Guobiao (Beijing) Testing & Certification Co., Ltd. The bones of bovine were bought from Weihai, China.

2.2. Batch Experiments. The adsorption performance was studied by batch equilibrium experiments. The initial concentration range of copper was 0–500 mg/L. 0.2 g hydroxyapatite was added into 30 mL copper solution for 72 h. The equilibrated suspensions were centrifuged for 5 min at 8000 rpm. Langmuir adsorption isotherm was utilized to simulate the adsorption behavior [54]. For adsorption kinetic, 0.2 g hydroxyapatite was added into a 30 mL copper solution for different reaction times. The pseudo-second-order kinetic model was used to fit the copper uptake kinetics on hydroxyapatite [55]. The above experiments for each condition were conducted in triplicates.

2.3. Column Experiment. The experiment used a glass column (length: 15.5 cm; inner diameter: 3.6 cm) equipped with sampling ports at the top. The column was packed with 20 g hydroxyapatite in the middle of the column together with quartz at the top and base of the column. In the column experiment, the 20 mg/L copper solution was pumped upward through the column at a constant flow rate of 0.612 mL/min to simulate a flow rate of 1 m/d for the groundwater environment. Detailed information regarding the column is presented in Table SI.1. The groundwater model software (FEFLOW 6.0) was carried out to simulate the results from the column experiment. The mathematical model was described as the one-dimensional of copper solution undergoing equilibrium sorption in porous hydroxyapatite column based on the adsorption mechanism.

2.4. Characterization of Hydroxyapatite before/after Adsorbing Copper. The thermogravimetric behavior of bovine bone was investigated through thermogravimetric-differential scanning calorimetry (Diamond TG-DSC, PE) at a heating rate of $10^{\circ}C/min$ under an air atmosphere. The

element content of hydroxyapatite was measured by X-ray Fluorescence Spectrometer (XRF, ZSX PrimusII). Nitrogen isotherms were investigated using ratio surface and porosity analyzer (BET, Autosorb-iQ). Surface areas were recorded through Brunnauer–Emmett–Teller (BET) equation fitting. Phase analysis was analyzed by powder X-ray diffractometer (XRD, SmartLab) from 5° to 120° with a step of 0.02, speed of 2°/min with Cu Kα radiation at 40 kV and 200 mA. Rietveld refinement of solids was conducted using FullProf software. Inductively coupled plasma atomic emission spectrometry (ICP-OES, ICAP 7600) was used for the determination of copper concentration. Surface chemical composition was measured through XPS (Thermo Scientific Escalab 250Xi+) equipped with an Al Kα X-ray as the excitation source, and the spectra binding energy was calibrated with the C 1s peak at 284.8 eV. Morphology and element distribution were speculated by a high-resolution transmission electron microscope (HRTEM, TalosF200X). The adsorption energy was calculated through the Materials Studio software package with the CASTEP module and ultrasoft pseudopotentials, where the energy cut-off was 520 eV, and the energy change was less than 1×10^{-6} eV. The optimized structure was adopted to make a (001) surface adsorption model with 14 Å thick bulk hydroxyapatite and a 24 Å thick vacuum layer. The vacuum distance (24 Å) is enough to avoid interaction between periodic configurations. DFT calculations were conducted under the Monkhorst–Pack k-mesh of $3 \times 3 \times 2$ in the Brillouin zone. The adsorption energy is as follows:

$$E\text{ads} = E(\text{Total}) - E(\text{HAP}) - E(\text{Cu}), \quad (1)$$

where $E(\text{Total})$ is the total energy of the hydroxyapatite adsorbing copper, $E(\text{HAP})$ is the energy of bulk hydroxyapatite, and $E(\text{Cu})$ is the energy of the isolated copper atom.

3. Results and Discussion

3.1. Effect of Calcination on the Hydroxyapatite.
Calcination temperature is a critical factor in determining the crystallinity, grain size, and pore structure of hydroxyapatite. To investigate the effect of calcination temperature on the bovine bone, comprehensive analyses are employed to discuss the hydroxyapatite formation from bovine bone. The thermogravimetric analysis is essential for investigating the hydroxyapatite extraction process from bovine bone (Figure 1(a)). A slight weight loss of 8% is attributed to the evaporation of adsorbed water at low temperatures (<120°C). The DSC curve shows a low endothermic peak correspondingly. The decomposition of organic matter causes a weight loss of 36.7% at 120–540°C. This reaction is followed by broad endothermic peaks correspondingly. A slight weight loss of 2.4% at 540–900°C can occur due to the dehydroxylation of hydroxyapatite promoted by heat.

To control the crystallinity and porosity, a series of characterizations systematically depict the crystallization process of the hydroxyapatite phase during the heat sintering. XRD analysis confirms that all powders under different sintering temperatures are hydroxyapatite (Ca$_{10}$(PO$_4$)$_6$(OH)$_2$,

JCPDS 84-1998). The crystallinity increases with increasing temperature due to the broad diffraction peaks transform into sharp diffraction peaks (Figure 1(b)). These results agree with previous reports [39, 41, 56]. In the process of heat treatment, the crystal phase of hydroxyapatite gradually emerges as the calcination temperature increases between 500°C and 600°C. The organic matter is decomposed into carbon dioxide through carbonation and decarboxylation. The nitrogen adsorption isotherms of hydroxyapatite under different temperatures belong to V-type adsorption isotherms, indicating that hydroxyapatite has a pore structure with the coexistence of micropores and mesopores (Figure 1(c)). The specific surface area, specific volume, and pore diameter also decrease with the increase in calcination temperature (Figure 1(d)). Specific surface area is 11.43 m^2/g under 600°C. XRF analysis confirms that hydroxyapatite under 600°C mainly consists of three components, containing calcium, oxygen, phosphorus (Table SI.2). Hence, 600°C is the suitable sintering temperature for hydroxyapatite derived from bovine bone.

3.2. Batch Experiment.
The adsorption amount as the function of copper concentration is shown in Figure 2(a). The adsorption capacity of 25.7 mg/g is superior to most of the adsorbents (Table 1) [53–64]. The copper adsorption isotherm agrees well with the Langmuir model interpreting as homogeneous monolayer adsorption. The detailed parameters are shown in Table SI.3. The R^2 value of the copper fitting model reaches 0.9993 (Figure 2(b)). The effect of contact time on the copper uptake is investigated to explore the reaction kinetic, which is shown in Figure 2(c). The adsorption process of copper by hydroxyapatite is fitting well with the pseudo-second-order kinetic model indicating the chemisorption. It can be found that the adsorption capacity of copper increases rapidly in the first 10 h. However, only a slight increase in adsorption capacity is observed after 10 h. It declares that its adsorption process consists of two parts: adsorption by available surface and further transformation from the solid-liquid interface to the pore of hydroxyapatite. The parameter values obtained through the pseudo-second-order kinetics model fitting are shown in Table SI.3. The R^2 value of copper fitting models is 0.9868 correspondingly (Figure 2(d)). It can be concluded that copper removal by hydroxyapatite is mainly rate-limited chemisorption.

3.3. Column Experiment.
The removal behavior of copper by hydroxyapatite is further evaluated by performing a column study. The breakthrough curve of copper for a column packed with hydroxyapatite is shown in Figure 3(a). At C/$C_0 = 0.5$, the number of pore volume (PV) is 450, suggesting excellent column durability [65]. Hydroxyapatite has a stable hydraulic performance to copper because no clogging phenomenon happened in the column. Based on the simulation model, the breakthrough curve of different copper concentrations has been further predicted through FEFLOW software (Figure 3(b)). The breakthrough time decreases with the increase in input copper concentration. The half-life of the reaction reaches 43 d when the input concentration of copper is 15 mg/L. The above results confirm that
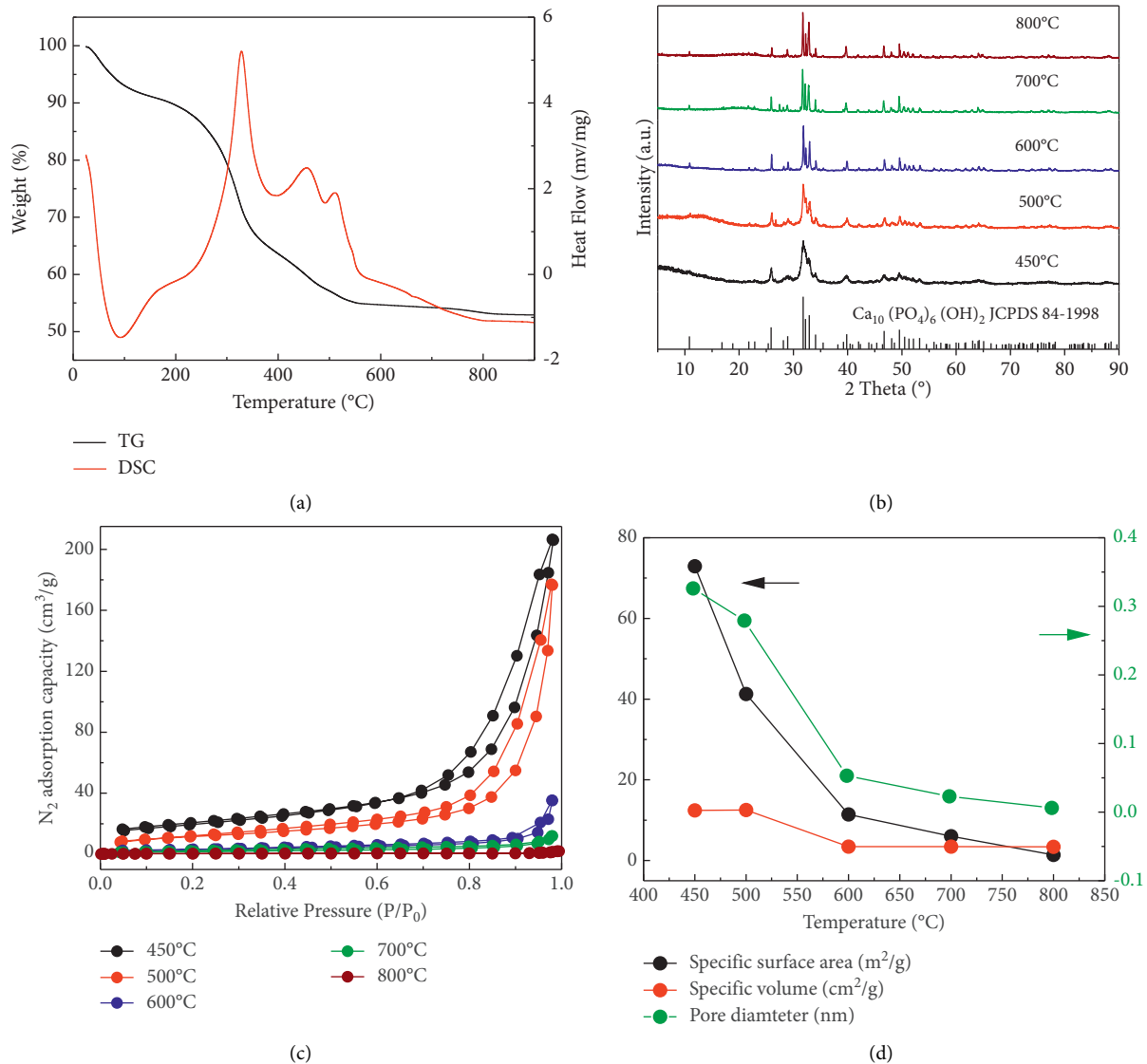
(a)

(b)

(c)

(d)

FIGURE 1: (a) TG-DSC curve of bovine bone. (b) XRD patterns of hydroxyapatite under different calcination temperatures. (c) N_2 adsorption isotherms of hydroxyapatite under different calcination temperatures. (d) Surface parameters of hydroxyapatite under different calcination temperatures.

hydroxyapatite derived from bovine bone is highly effective in in situ remediation of copper-contaminated groundwater as a suitable filling material within PRB. This dynamic column study provides a good prospect for removing copper in field application.

3.4. Adsorption Mechanism.

XRD combined with Rietveld refinement is used to analyze the product after adsorption shown in Figure 4(a). The result represents that the product after adsorbing copper belongs to hydroxyapatite phase $(Ca_{10}(PO_4)_6(OH)_2)$ according to JCPDS 84-1998. Rietveld refinement defines that the calcium site and phosphate site were fully occupied. The fitting coefficients are R_p of 9.61% and R_{wp} of 13.5%. The functional groups of hydroxyapatites before/after adsorbing copper are identified through FTIR analysis, and corresponding results are presented in Figure 4(b). It can

be seen that characteristic peak of hydroxyapatite before/after adsorbing copper is approximately identical. The hydroxyl stretching vibration band at $3560 \, cm^{-1}$ is presented. The characteristic peaks at $1030 \, cm^{-1}$, $609 \, cm^{-1}$, and $545 \, cm^{-1}$ are attributed to asymmetric stretching of PO_4^{3-}. Besides, the carbonate group is observed at $1407 \, cm^{-1}$, which indicates slight substitution of carbonate group into phosphate group in the hydroxyapatite lattice.

XPS analysis (Figure 5) is consistent with the XRD data. The fitted Cu 2p spectra (Figure 5(a)) show two peaks of Cu $2p_{1/2}$ and Cu $2p_{3/2}$ at the binding energy of 953.25 eV and 933.5 eV, respectively [66]. The spin-orbit splitting $E(Cu \, 2p_{1/2}) - E(Cu \, 2p_{3/2})$ of 19.73 eV is associated with the Cu^{2+}. The XPS characterization is corresponding to the presence of copper ions adsorbed on the surface of hydroxyapatite. The XPS spectra of Ca 2p, P 2p, and O 1s are characteristic of phosphorus, calcium, and oxygen ions in hydroxyapatite before/after adsorbing
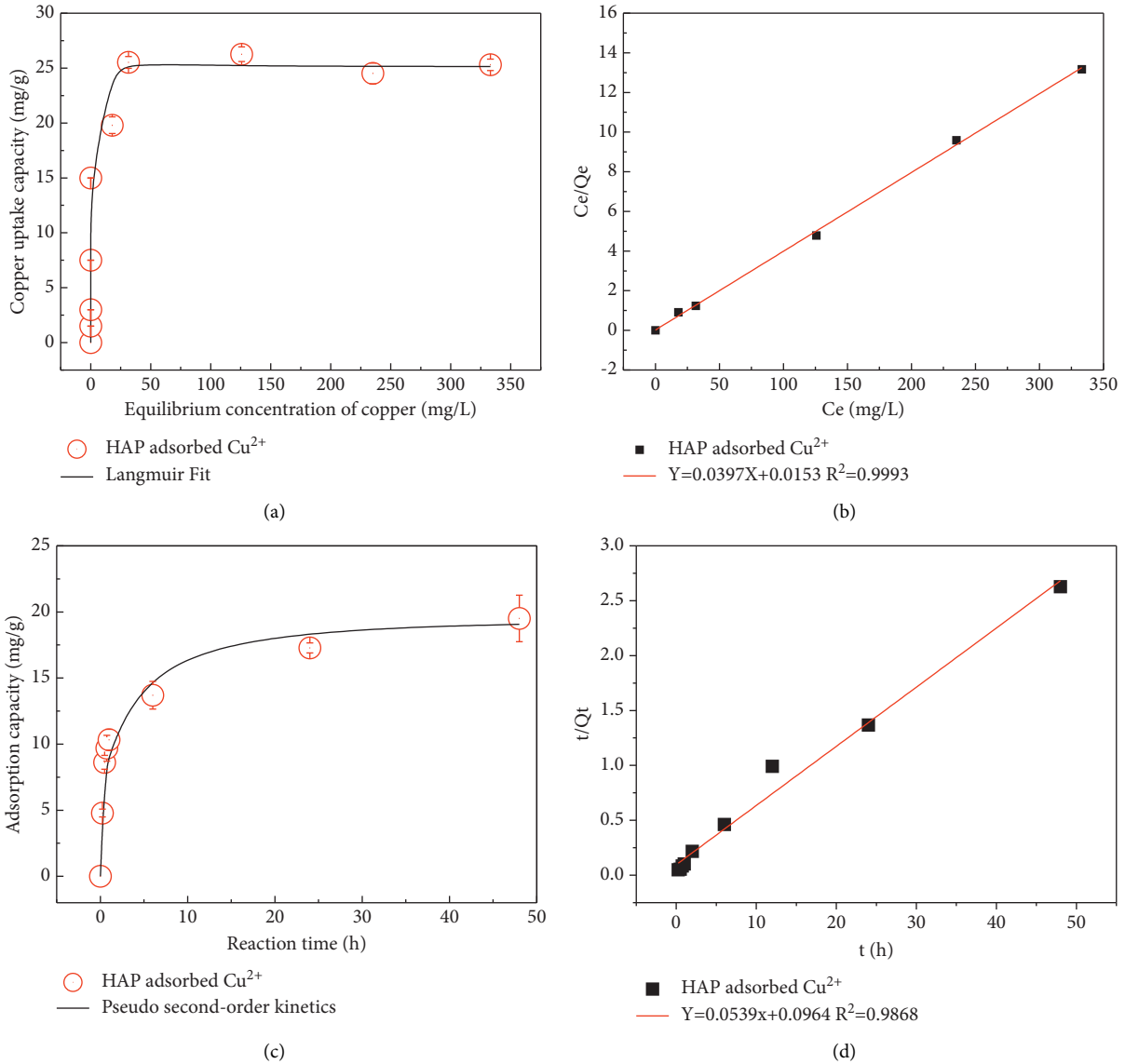
(a)

(b)

(c)

(d)

FIGURE 2: (a) Adsorption equilibrium isotherm of copper on hydroxyapatite. Langmuir model fitting. (b) Linear plot of Langmuir model for adsorption isotherm. (c) Adsorption kinetic of copper on hydroxyapatite. Pseudo-second-order kinetic model fitting (adsorbent dosage: 0.2 g; copper concentration: 500 mg/L; solid/solution ratio: 6.7 g/L at $25 \pm 2°C$). (d) Linear plot of pseudo-second-order kinetic model for adsorption kinetics.

TABLE 1: Adsorption capacity of copper by various absorbent.

| Adsorbent	Q_m(mg/g)	References
Raw pomegranate peel	30.12	Ben-Ali et al. 2017 [57]
Pine fruit	14.1	Najim et al. 2009 [58]
$Fe_5C_2@SiO_2$	37.73	Ahmadpoor et al. 2019 [59]
Bioball	5.60	Çelebi 2021[60]
Chicken feather	7.84	Solis-Moreno et al. 2021 [61]
Chicken bone charcoal	15.057	Niu et al. 2021 [62]
Activated carbon	13.05	Imamoglu and Tekir 2008 [63]
Rice shell	2.954	Aydin et al. 2008 [64]
Hydroxyapatite	25.7	Present study

(a)

(b)
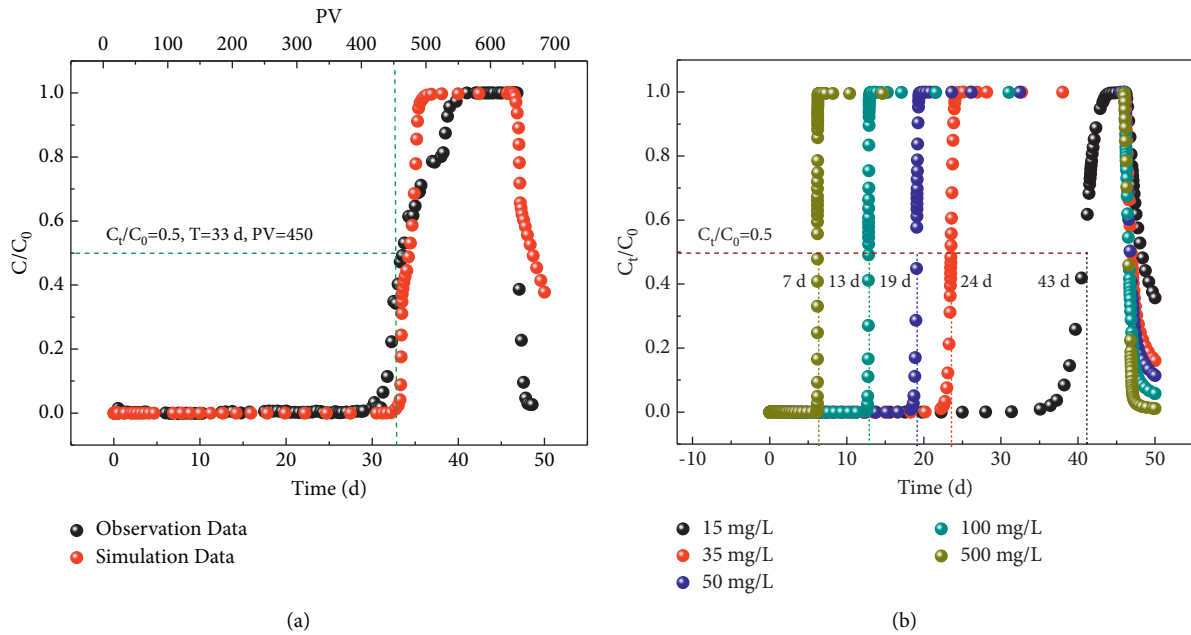
FIGURE 3: (a) Experimental and fitting breakthrough curve of copper for a column packed with hydroxyapatite. The input concentration of copper is 20 mg/L. Adsorbent mass is 20 g. (b) Predicting breakthrough curve of copper for a column packed with hydroxyapatite for different copper concentrations.
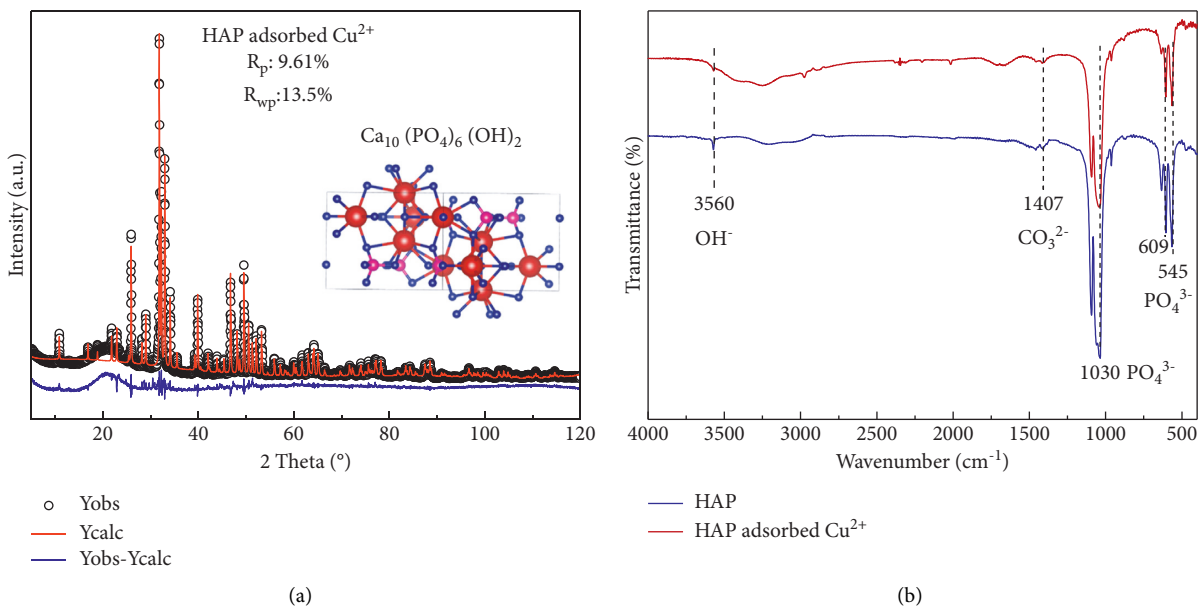

(a)

(b)

FIGURE 4: (a) X-ray diffraction patterns with Rietveld refinement of hydroxyapatite adsorbing copper. (b) FTIR spectra before/after adsorbing copper by hydroxyapatite.

copper (Figures 5(c) and 5(d)). The P 2p peaks at 133.8 eV and 132.9 eV are assigned to P of hydroxyapatite ($Ca_{10}(PO_4)_6(OH)_2$). The Ca 2p spectra are composed by two peaks Ca $2p_{1/2}$ and Ca $2p_{3/2}$, in which the energy separation value of $E(Ca\ 2p_{1/2}) - E(Ca\ 2p_{3/2})$ is 3.57 eV on representing of Ca^{2+} ions. The binding energy of O 1s consists of two peaks at 531.58 eV and 530.85 eV associated with the presence of O-P and O-H groups in hydroxyapatite, respectively. The XPS results also show the similar surface chemical status of hydroxyapatite before/after adsorbing copper.

Morphology characterization further confirms that copper is adsorbed on the surface of nanorod hydroxyapatite in Figure 6. HRTEM images with annular dark field (HADDF-HRTEM) of hydroxyapatite adsorbing copper show complete nanorods. The corresponding EDX elemental mappings also show the core/shell structure formation. Copper is mostly located in the outside area of the nanorod structure. Furthermore, calcium, oxygen, and phosphorus are uniformly distributed on the internal area of the nanostructure. The above results confirm that surface
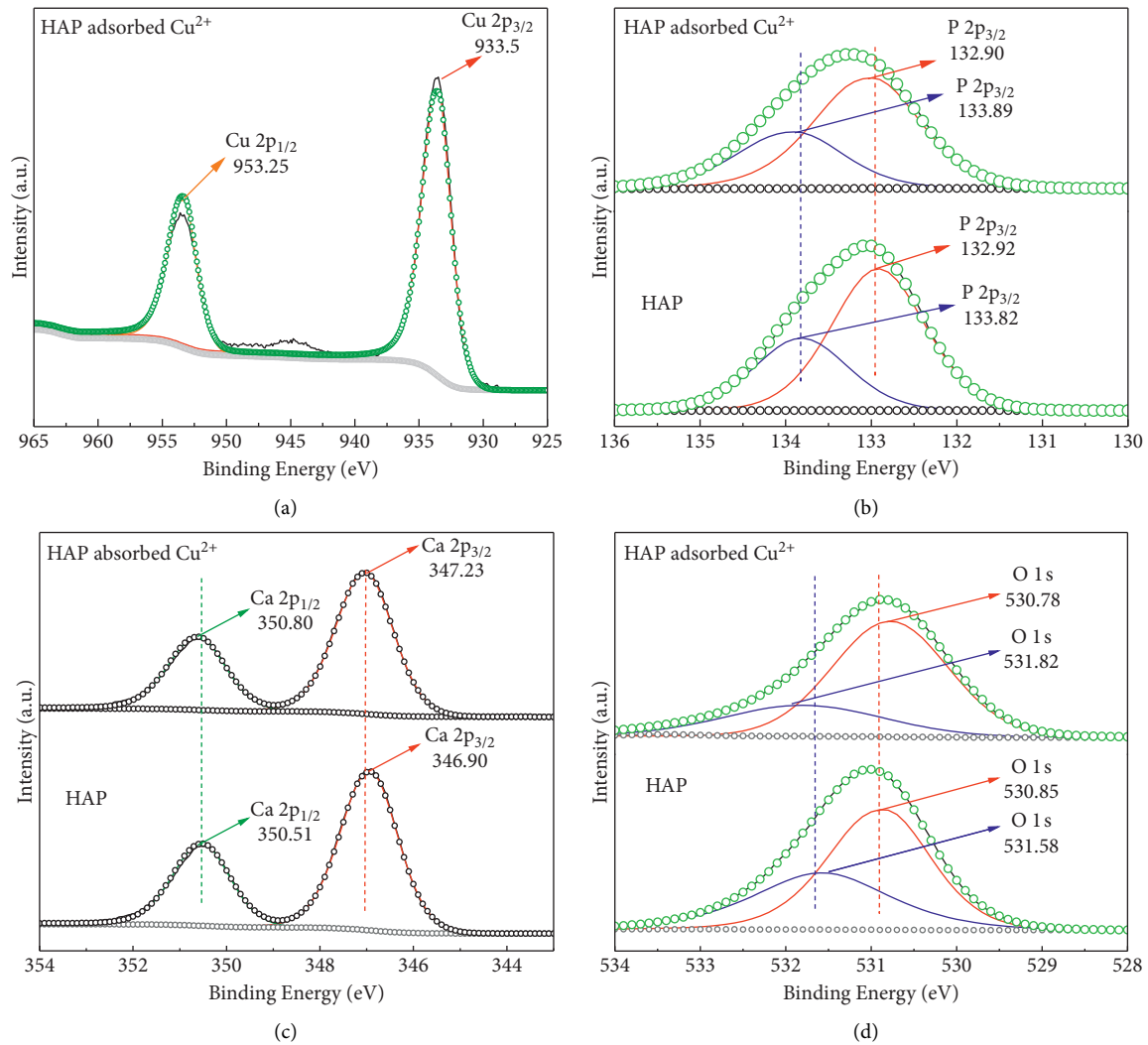
FIGURE 5: XPS spectra before/after adsorbing copper by hydroxyapatite. (a) Cu 2p XPS spectra. (b) P 2p XPS spectra. (c) Ca 2p XPS spectra. (d) O 1s XPS spectra.
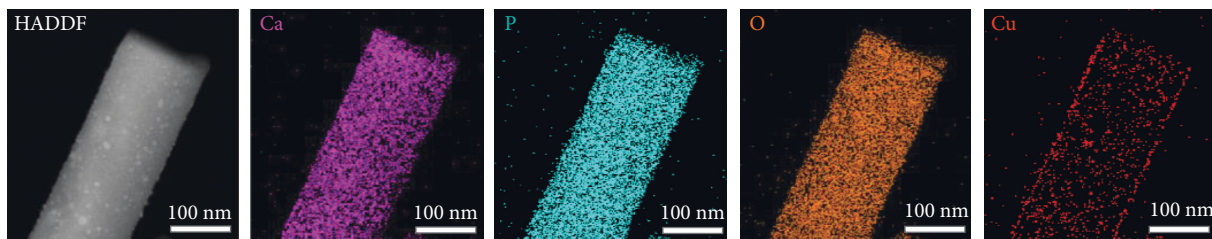

FIGURE 6: HADDF-STEM image and EDX elemental mappings of hydroxyapatite after adsorbing copper.

chemisorption is the copper uptake mechanism on hydroxyapatite.

DFT calculation is conducted to further study the adsorption site in Figure 7. (001) and (100) are typical planes in hydroxyapatite, in which hydroxyapatite has electronegativity in (001) and electropositivity in (100). Bivalent cation is easier to be adsorbed on hydroxyapatite (001) surface through electrostatic attraction. Hence, (001) plane is considered as a dominant plane. Hydroxyapatite has acidic-basic sites, where acidic groups ($\equiv$POH, $\equiv$PO⁻, and $\equiv$CaOH) could complex with

heavy metal on the surface. The calculation result shows that copper prefers to be adsorbed to the Ca(I) site through bonding to three oxygens of phosphate group stably in the hydroxyapatite (001). The calculation adsorption energy before/after adsorbing copper is $-1.15\,eV$, indicating strong copper adsorption on the surface. Hence, a surface chemisorption model has proposed that copper bounds to the oxygen of phosphate through complexation with a Cu-O distance of ~2.15 Å. The DFT calculations provide new insights into the copper adsorption mechanism on hydroxyapatite as adsorbent.
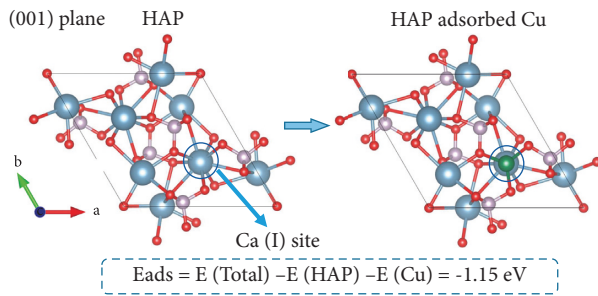
FIGURE 7: DFT calculation of copper adsorption energy on hydroxyapatite. Copper adsorption on the pristine hydroxyapatite (001). Oxygen, calcium, phosphorus, hydrogen, and copper are in red, blue, pink, yellow, and green, respectively.

4. Conclusion

Copper-contaminated groundwater is directly associated with human health and the ecological environment. In this paper, cost-effective hydroxyapatite derived from bovine bone was proven as a suitable adsorbent for in situ remediation of copper-contaminated groundwater within PRB. Calcination temperature has a significant effect on the crystallinity and porosity, and 600°C is confirmed as suitable temperature for hydroxyapatite derived from the bovine bone. Hydroxyapatite has a porous structure, and its specific surface area is $11.43 \, m^2/g$. Hydroxyapatite is proven as an excellent adsorbent owing to cost-effectiveness, great adsorption capacity, and longevity. Adsorption isotherm is represented by the Langmuir isotherm model, and adsorption capacity of 25.7 mg/g is superior to most of the adsorbents. The kinetic study is accurately fitted by the pseudo-second-order kinetic model interpreted with chemical reaction. In addition, column study confirms that hydroxyapatite has excellent hydraulic performance with no clogging phenomenon happened. At $C/C_0 = 0.5$, the number of pore volume (PV) reaches 450, suggesting stable durability. The model predicates that breakthrough time decreases with the increase in input copper concentration through FEFLOW software. The batch and column experiments also reveal that the overall adsorption process follows up the monolayer chemisorption. XRD combined with Rietveld refinement demonstrated that copper has not incorporated into the calcium sites in hydroxyapatite. Other characterizations such as XPS analysis, EDX mapping images, and FTIR further confirm that copper is adsorbed on the surface of hydroxyapatite. DFT calculation shows that copper was attracted to oxygen atoms to form complexes based on the phosphate group in the (001) plane. The adsorption energy is $-1.15 \, eV$ with a Cu-O distance of ~2.15 Å. This work provides an alternative strategy as filling material for in situ remediation of copper-contaminated groundwater and enriches relevant theoretical references.

Data Availability

The data used to support the findings of this study are available from the corresponding author upon request.

Conflicts of Interest

The authors declare that there are no conflicts of interest regarding the publication of this paper.

Acknowledgments

Supplementary Materials

The supporting information is available free of charge. Additional tables are displayed in the supplementary materials file, including parameters for the column experiment, mass fraction of hydroxyapatite, and detailed parameters of copper adsorption. The data used and generated in this paper are openly available. (*Supplementary Materials*)

References

[1] N. Moosdorf and T. Oehler, "Societal use of fresh submarine groundwater discharge: An overlooked water resource," *Earth-Science Reviews*, vol. 171, pp. 338–348, 2017.

[2] X. Gong, Z. Chen, and Z. Luo, "Spatial distribution, temporal variation, and sources of heavy metal pollution in groundwater of a century-old nonferrous metal mining and smelting area in China," *Environmental Monitoring and Assessment*, vol. 186, no. 12, pp. 9101–9116, 2014.

[3] Y. Fan, T. Zhu, M. Li, J. He, and R. Huang, "Heavy Metal contamination in soil and Brown Rice and human health Risk Assessment near three Mining Areas in Central China," *Journal Of Healthcare Engineering*, vol. 2017, Article ID 4124302, 9 pages, 2017.

[4] E. M. Alissa and G. A. Ferns, "Heavy metal poisoning and cardiovascular disease," *Journal of Toxicology*, vol. 2011, Article ID 870125, 21 pages, 2011.

[5] R. W. Gaikwad, S. A. Misal, and D. V. Gupta, "Removal of metal from acid mine drainage (AMD) by using natural zeolite of Nizarneshwar Hills of Western India," *Arabian Journal of Geosciences*, vol. 4, no. 1-2, pp. 85–89, 2009.

[6] I. Panfili, M. L. Bartucca, E. Ballerini, and D. Del Buono, "Combination of aquatic species and safeners improves the remediation of copper polluted water," *Science of the Total Environment*, vol. 601-602, pp. 1263–1270, 2017.

[7] H. Sun, L. Sun, Y. Zhao et al., "A combined hydrate-based method for removing heavy metals from simulated wastewater with high concentrations," *Journal of Environmental Chemical Engineering*, vol. 9, no. 6, Article ID 106633, 2021.

[8] General Administration of Quality Supervision, *Inspection and Quarantine of the People's Republic of China, GB 25467-2010 Emission Standard of Pollutants for Copper, Nickel, Cobalt Industry*, China Environmental Science Press, Beijing, China, 2013.

[9] ISO, *Soil Quality, Extraction of Trace Elements Soluble in Aqua Regia*, ISO 11466, Geneva, Switzerland, 1995.

[10] N. Makombe and R. D. Gwisai, "Soil remediation Practices for Hydrocarbon and heavy Metal Reclamation in Mining polluted soils," *The Scientific World Journal*, vol. 2018, Article ID 5130430, 7 pages, 2018.

[11] F. Feizi, A. K. Sarmah, and R. Rangsivek, "Adsorption of pharmaceuticals in a fixed-bed column using tyre-based activated carbon: experimental investigations and numerical

modelling," *Journal of Hazardous Materials*, vol. 417, Article ID 126010, 2021.

[12] B. Thangagiri, A. Sakthivel, K. Jeyasubramanian, S. Seenivasan, J. Dhaveethu Raja, and K. Yun, "Removal of hexavalent chromium by biochar derived from Azadirachta indica leaves: batch and column studies," *Chemosphere*, vol. 286, no. Pt 1, Article ID 131598, 2022.

[13] Y. Zha, T.-C. J. Yeh, W. A. Illman, C. M. W. Tso, C.-H. M. Carrera, and Y.-L. Wang, "Exploitation of pump-and-treat remediation systems for characterization of hydraulic heterogeneity," *Journal of Hydrology*, vol. 573, pp. 324–340, 2019.

[14] J. Song, G. Huang, D. Han, Q. Hou, L. Gan, and M. Zhang, "A review of reactive media within permeable reactive barriers for the removal of heavy metal(loid)s in groundwater: Current status and future prospects," *Journal of Cleaner Production*, vol. 319, 2021.

[15] J. Lee, A. J. Graettinger, J. Moylan, and H. W. Reeves, "Directed site exploration for permeable reactive barrier design," *Journal of Hazardous Materials*, vol. 162, no. 1, pp. 222–229, 2009.

[16] H. Zhou, Z. Liu, X. Li, and J. Xu, "Remediation of lead (II)-contaminated soil using electrokinetics assisted by permeable reactive barrier with different filling materials," *Journal of Hazardous Materials*, vol. 408, Article ID 124885, 2021.

[17] B. Yu, Z. Chen, and J. Wu, "Experimental investigation on seepage stability of filling Material of Karst Collapse Pillar in Mining Engineering," *Advances in Civil Engineering*, vol. 2018, Article ID 3986490, 10 pages, 2018.

[18] F. Zhu, X. Tan, W. Zhao et al., "Efficiency assessment of ZVI-based media as fillers in permeable reactive barrier for multiple heavy metal-contaminated groundwater remediation," *Journal of Hazardous Materials*, vol. 424, 2022.

[19] J. Oliva, J. De Pablo, J.-L. Cortina, and C. Ayora, "Removal of cadmium, copper, nickel, cobalt and mercury from water by Apatite II: column experiments," *Journal of Hazardous Materials*, vol. 194, pp. 312–323, 2011.

[20] C. Rojas-Mayorga, D. Mendoza-Castillo, A. Bonilla-Petriciolet, and J. Silvestre-Albero, "Tailoring the adsorption behavior of bone char for heavy metal removal from aqueous solution," *Adsorption Science and Technology*, vol. 34, no. 6, pp. 368–387, 2016.

[21] C. Xue, L. Zhu, S. Lei et al., "Lead competition alters the zinc adsorption mechanism on animal-derived biochar," *Science of the Total Environment*, vol. 713, Article ID 136395, 2020.

[22] Y.-Y. Wang, Y.-X. Liu, H.-H. Lu, R.-Q. Yang, and S.-M. Yang, "Competitive adsorption of Pb(II), Cu(II), and Zn(II) ions onto hydroxyapatite-biochar nanocomposite in aqueous solutions," *Journal of Solid State Chemistry*, vol. 261, pp. 53–61, 2018.

[23] S. Lei, Y. Shi, Y. Qiu, L. Che, and C. Xue, "Performance and mechanisms of emerging animal-derived biochars for immobilization of heavy metals," *Science of the Total Environment*, vol. 646, pp. 1281–1289, 2019.

[24] D. Smoleń, T. Chudoba, S. Gierlotka et al., "Hydroxyapatite Nanopowder synthesis with a Programmed Resorption rate," *Journal of Nanomaterials*, vol. 2012, Article ID 841971, 9 pages, 2012.

[25] J. M. Hughes and J. F. Rakovan, "Structurally Robust, chemically Diverse: Apatite and Apatite Supergroup Minerals," *Elements*, vol. 11, no. 3, pp. 165–170, 2015.

[26] Y. Wang, R. Li, W. Liu, L. Cheng, Q. Jiang, and Y. Zhang, "Exploratory of immobilization remediation of hydroxyapatite (HAP) on lead-contaminated soils," *Environmental*

Science and Pollution Research, vol. 26, no. 26, pp. 26674–26684, 2019.

[27] A. M. Mohammad, T. A. Salah Eldin, M. A. Hassan, and B. E. El-Anadouli, "Efficient treatment of lead-containing wastewater by hydroxyapatite/chitosan nanostructures," *Arabian Journal of Chemistry*, vol. 10, no. 5, pp. 683–690, 2017.

[28] L. Dong, Z. Zhu, Y. Qiu, and J. Zhao, "Removal of lead from aqueous solution by hydroxyapatite/magnetite composite adsorbent," *Chemical Engineering Journal*, vol. 165, no. 3, pp. 827–834, 2010.

[29] F. Safatian, Z. Doago, M. Torabbeigi, H. Rahmani Shams, and N. Ahadi, "Lead ion removal from water by hydroxyapatite nanostructures synthesized from egg sells with microwave irradiation," *Applied Water Science*, vol. 9, no. 4, p. 108, 2019.

[30] W. Zhang, H. Liu, X. Fan, Z. Zhuo, and Y. Guo, "Removal of uranium from aqueous solution by a permeable reactive barrier loaded with hydroxyapatite-coated quartz sand: Implication for groundwater remediation," *Geochemistry*, vol. 80, no. 4, 2020.

[31] S. A. Chattanathan, T. P. Clement, S. R. Kanel, M. O. Barnett, and N. Chatakondi, "Remediation of uranium-contaminated groundwater by sorption onto hydroxyapatite derived from Catfish bones," *Water, Air, & Soil Pollution*, vol. 224, no. 2, p. 1429, 2013.

[32] C. C. Fuller, J. R. Bargar, J. A. Davis, and M. J. Piana, "Mechanisms of uranium interactions with hydroxyapatite: Implications for groundwater remediation," *Environmental Science & Technology*, vol. 36, no. 2, pp. 158–165, 2002.

[33] Y. Liu, R. Zhang, Z. Sun et al., "Remediation of artificially contaminated soil and groundwater with copper using hydroxyapatite/calcium silicate hydrate recovered from phosphorus-rich wastewater," *Environmental Pollution*, vol. 272, Article ID 115978, 2021.

[34] P. R. Rad and A. Fazlali, "Optimization of permeable reactive barrier dimensions and location in groundwater remediation contaminated by landfill pollution," *Journal of Water Process Engineering*, vol. 35, 2020.

[35] C. Stotzel, F. A. Muller, F. Reinert, F. Niederdraenk, J. Barralet, and U. Gbureck, "Ion adsorption behaviour of hydroxyapatite with different crystallinities," *Colloids and Surfaces B: Biointerfaces*, vol. 74, no. 1, pp. 91–95, 2009.

[36] Y. X. Pang and X. Bao, "Influence of temperature, ripening time and calcination on the morphology and crystallinity of hydroxyapatite nanoparticles," *Journal of the European Ceramic Society*, vol. 23, no. 10, pp. 1697–1704, 2003.

[37] P. T. Ngueagni, E. D. Woumfo, P. S. Kumar et al., "Adsorption of Cu(II) ions by modified horn core: effect of temperature on adsorbent preparation and extended application in river water," *Journal of Molecular Liquids*, vol. 298, 2020.

[38] M. Wang, Y. Liu, Y. Yao, L. Han, and X. Liu, "Comparative evaluation of bone chars derived from bovine parts: Physicochemical properties and copper sorption behavior," *Science of the Total Environment*, vol. 700, Article ID 134470, 2020.

[39] P. P. Biswas, B. Liang, G. Turner-Walker et al., "Systematic changes of bone hydroxyapatite along a charring temperature gradient: An integrative study with dissolution behavior," *Science of the Total Environment*, vol. 766, Article ID 142601, 2021.

[40] S. Patel, J. Han, W. Qiu, and W. Gao, "Synthesis and characterisation of mesoporous bone char obtained by pyrolysis of animal bones, for environmental application," *Journal of Environmental Chemical Engineering*, vol. 3, no. 4, pp. 2368–2377, 2015.

[41] A. M. Sofronia, R. Baies, E. M. Anghel, C. A. Marinescu, and S. Tanasescu, "Thermal and structural characterization of synthetic and natural nanocrystalline hydroxyapatite," *Materials Science and Engineering: C*, vol. 43, pp. 153–163, 2014.

[42] W. P. Wijesinghe, M. M. Mantilaka, E. V. Premalal et al., "Facile synthesis of both needle-like and spherical hydroxyapatite nanoparticles: effect of synthetic temperature and calcination on morphology, crystallite size and crystallinity," *Materials Science and Engineering: C*, vol. 42, pp. 83–90, 2014.

[43] Z. Li, M.-M. Zhou, and W. Lin, "The research of Nanoparticle and Microparticle hydroxyapatite Amendment in Multiple heavy Metals contaminated soil remediation," *Journal of Nanomaterials*, vol. 2014, Article ID 168418, 8 pages, 2014.

[44] R. Agha Beygli, N. Mohaghegh, and E. Rahimi, "Metal ion adsorption from wastewater by g-C$_3$N$_4$ modified with hydroxyapatite: a case study from Sarcheshmeh Acid Mine Drainage," *Research on Chemical Intermediates*, vol. 45, no. 4, pp. 2255–2268, 2019.

[45] Y. Chen, M. Li, Y. Li et al., "Hydroxyapatite modified sludge-based biochar for the adsorption of Cu^{2+} and Cd^{2+}: Adsorption behavior and mechanisms," *Bioresource Technology*, vol. 321, Article ID 124413, 2021.

[46] D. N. Thanh, P. Novák, J. Vejpravova, H. N. Vu, J. Lederer, and T. Munshi, "Removal of copper and nickel from water using nanocomposite of magnetic hydroxyapatite nanorods," *Journal of Magnetism and Magnetic Materials*, vol. 456, pp. 451–460, 2018.

[47] E.-S. Bogya, R. Barabás, A. Csavdári, V. Dejeu, and I. Baldea, "Hydroxyapatite modified with silica used for sorption of copper(II)," *Chemical Papers*, vol. 63, no. 5, 2009.

[48] Y. Zhan, J. Lin, and J. Li, "Preparation and characterization of surfactant-modified hydroxyapatite/zeolite composite and its adsorption behavior toward humic acid and copper(II)," *Environmental Science and Pollution Research*, vol. 20, no. 4, pp. 2512–2526, 2013.

[49] P. Li, X. Li, and S. Dai, "Adsorption of gold cyanide on quartz," *Colloids and Surfaces A: Physicochemical and Engineering Aspects*, vol. 590, 2020.

[50] X.-Y. Liu, J.-W. Cao, X.-L. Qin et al., "A Computational Validation of water Molecules Adsorption on an NaCl surface," *Crystals*, vol. 11, no. 6, p. 610, 2021.

[51] M.-H. Ri, Y.-M. Jang, U.-S. Ri, C. J. Yu, K. I. Kim, and S. U. Kim, "Ab initio investigation of Adsorption characteristics of Bisphosphonates on hydroxyapatite (001) surface," *Journal of Materials Science*, vol. 53, no. 6, pp. 4252–4261, 2017.

[52] A. Fahami, B. Nasiri-Tabrizi, G. W. Beall, and W. J. Basirun, "Structural insights of mechanically induced aluminum-doped hydroxyapatite nanoparticles by Rietveld refinement," *Chinese Journal of Chemical Engineering*, vol. 25, no. 2, pp. 238–247, 2017.

[53] S. Lala, M. Ghosh, P. K. Das, D. Das, T. Kar, and S. Pradhan, "Magnesium substitution in carbonated hydroxyapatite: structural and microstructural characterization by Rietveld's refinement," *Materials Chemistry and Physics*, vol. 170, pp. 319–329, 2016.

[54] S. L. Iconaru, M. Motelica-Heino, R. Guegan, M. Beuran, A. Costescu, and D. Predoi, "Adsorption of Pb (II) ions onto hydroxyapatite Nanopowders in Aqueous solutions," *Materials*, vol. 11, pp. 2204–11, 2018.

[55] Y. Long, J. Jiang, J. Hu, X. Hu, Q. Yang, and S. Zhou, "Removal of Pb(II) from aqueous solution by hydroxyapatite/carbon composite: preparation and adsorption behavior,"

[56] *Colloids and Surfaces A: Physicochemical and Engineering Aspects*, vol. 577, pp. 471–479, 2019.

[56] M. Younesi, S. Javadpour, and M. E. Bahrololoom, "Effect of heat treatment temperature on chemical compositions of extracted hydroxyapatite from bovine bone Ash," *Journal of Materials Engineering and Performance*, vol. 20, no. 8, pp. 1484–1490, 2011.

[57] S. Ben-Ali, I. Jaouali, S. Souissi-Najar, and A. Ouederni, "Characterization and adsorption capacity of raw pomegranate peel biosorbent for copper removal," *Journal of Cleaner Production*, vol. 142, pp. 3809–3821, 2017.

[58] T. S. Najim, N. J. Elais, and A. A. Dawood, "Adsorption of copper and iron using low cost Material as Adsorbent," *E-Journal of Chemistry*, vol. 6, no. 1, pp. 161–168, 2009.

[59] F. Ahmadpoor, S. A. Shojaosadati, and S. Z. Mousavi, "Magnetic silica coated iron carbide/alginate beads: synthesis and application for adsorption of Cu (II) from aqueous solutions," *International Journal of Biological Macromolecules*, vol. 128, pp. 941–947, 2019.

[60] H. Çelebi, "Use of Bioballs as an Adsorbent for the removal of copper," *Journal of the Chemical Society of Pakistan*, vol. 43, no. 2, p. 114, 2021.

[61] C. A. Solis-Moreno, E. Cervantes-Gonzalez, and M. Z. Saavedra-Leos, "Use and treatment of chicken feathers as a natural adsorbent for the removal of copper in aqueous solution," *Journal of Environmental Health Science and Engineering*, vol. 19, no. 1, pp. 707–720, 2021.

[62] C. Niu, S. Li, G. Zhou, Y. Wang, X. Dong, and X. Cao, "Preparation and characterization of magnetic modified bone charcoal for removing Cu^{2+} ions from industrial and mining wastewater," *Journal of Environmental Management*, vol. 297, Article ID 113221, 2021.

[63] M. Imamoglu and O. Tekir, "Removal of copper (II) and lead (II) ions from aqueous solutions by adsorption on activated carbon from a new precursor hazelnut husks," *Desalination*, vol. 228, no. 1–3, pp. 108–113, 2008.

[64] H. Aydin, Y. Bulut, and C. Yerlikaya, "Removal of copper (II) from aqueous solution by adsorption onto low-cost adsorbents," *Journal of Environmental Management*, vol. 87, no. 1, pp. 37–45, 2008.

[65] G. Du, Z. Li, L. Liao et al., "Cr(VI) retention and transport through Fe(III)-coated natural zeolite," *Journal of Hazardous Materials*, vol. 221-222, pp. 118–123, 2012.

[66] A. Amedlous, O. Amadine, Y. Essamlali, H. Maati, N. Semlal, and M. Zahouily, "Copper loaded hydroxyapatite nanoparticles as eco-friendly Fenton-like catalyst to effectively Remove organic Dyes," *Journal of Environmental Chemical Engineering*, vol. 9, no. 4, 2021.